Journal of Fluids and Structures (1997) **11,** 3–31

OSCILLATING RECTANGULAR AND OCTAGONAL PROFILES: INTERACTION OF LEADING- AND TRAILING-EDGE VORTEX FORMATION

S. DENIZ

Massachusetts Institute of Technology, Department of Aeronautics and Astronautics, Gas Turbine Laboratory, Cambridge, MA 02139, U.S.A.

AND

TH. STAUBLI

Swiss Federal Institute of Technology, Institute of Energy Technology, Turbomachinery Laboratory, CH-8092 Zurich, Switzerland

(Received 22 November 1995 and in revised form 12 August 1996)

Force measurements and flow visualization for transversely oscillating rectangular and octagonal profiles are presented. Flow fields are analysed, classified and related to the fluid forces and to the type of excitation of eventual fluid-elastic oscillations. The interaction of instability-induced and movement-induced excitation is shown, as well as the interaction of impinging leading-edge and trailing-edge vortices. The mechanisms leading to an energy transfer from the fluid to the body are associated with the phase shift of the fluctuating lift forces relative to the body oscillation. The abrupt change of phasing, observed within the range of synchronization of body motion and vortex shedding, is explained by an alteration of the timing in the formation of the synchronized vortices at the trailing-edge. Aspects of resonance and annihilation of lift forces are discussed with respect to the formation of vertical structures at the leading- and trailing-edge.

1. INTRODUCTION

THE OSCILLATION OF A BODY IN A FLOWING FLUID creates a time-dependent, three-dimensional flow field which in turn gives rise to the fluctuating pressure field on the surface of the body, involving most complex fluid/structure interactions. This is true for airfoils and even more for bluff bodies. Bearman (1985) calls it ''one of the most complicated but most challenging problems in fluid mechanics''; a statement which can be confirmed a decade later, more than ever. Many basic aspects of bluff-body fluid dynamics have been uncovered through their interaction with the body oscillation and much effort has been devoted to finding the correlation between excitation force and flow characteristics (Naudascher & Rockwell 1994). It is of great importance to understand the fluid dynamic mechanism of bluff body-vortex excitation, if one wants to predict, control and eventually suppress exciting forces (Rockwell 1990).

A first step for the synthesis of such fluid-dynamic problems becomes possible through classification of the predominant effects. In the following, classifications employed by Naudascher & Rockwell (1994) are briefly summarized because they will be used in the discussion of the experimental findings described in this paper. Naudascher & Rockwell distinguish three types of flow-induced excitation:

0889–9746/97/010003 + 29 $25.00/fl960065

EIE: Extraneously induced excitation (e.g. turbulent buffeting, periodic pulsation of oncoming flow);

IIE: Instability-induced excitation (flow instability inherent to the flow created by the structure under consideration), e.g. excitation induced by the von Kármán street;

MIE: Movement-induced excitation (fluid forces arising from the movement of the body or eventually of a fluid oscillator), e.g. galloping.

Frequently, the excitation of flow-induced vibration in a real system is complex in a sense that EIE, IIE, and MIE can be present simultaneously.

Further classification of one important group of IIE concerns the type of wake formation behind prismatic bodies (Naudascher & Wang 1993; see also Figure 2):

LEVS: Leading-edge vortex shedding (flow separation at the leading-edge and formation of vortices which dominate the near wake of the body);

ILEV: Impinging leading-edge vortices (flow separation at the leading-edge and impingement of the leading-edge vortices at the side surfaces and/or edges of the body);

TEVS: Trailing-edge vortex shedding (decisive flow separation at the trailing-edge and vortex-shedding analogue to the von Kármán street behind circular cylinders);

AEVS: Alternate-edge vortex shedding (vortex shedding occurring in a critical range of incidence where alternatingly one vortex separates at the leading-edge and the other at the trailing-edge).

The most important physical parameter of a two-dimensional body subjected to vortex-induced (IIE) or galloping (MIE) oscillation is the size and shape of its afterbody, that is the part of the cross-section downstream of the separation points (Parkinson 1989). For vortex-induced or galloping type of excitation, the pressure loading occurs principally on the afterbody surface. Accordingly, a body with a very short afterbody will only weakly be excited to oscillations. Thus a semicircular cylinder (D-section) will exhibit both vortex-induced oscillation and galloping, if a sufficient initial transverse velocity is given, when the flat face is upstream and normal to the incident flow. In this case the flow separates at the sharp edges and the semicircular cylinder forms the afterbody. If, however, the flat face is downstream, the flow will still separate at the edges, but now there is no afterbody. The cylinder is then stable exhibiting neither vortex-induced oscillation nor galloping (Parkinson 1974).

Figure 1 from Chaix (1972) demonstrates how dramatically the size of the afterbody may change with minor geometrical modification. A well developed von Kármán vortex street (TEVS) in the wake of an octagonal profile is observed in Figure 1(a). For this profile with a wedge angle of $\beta = 10°$, the flow initially separates at the leading-edge and then reattached, and finally separates at the trailing-edge [Figure 1(b)]. Increasing the wedge angle to $\beta = 16°$ [Figure 1(c)], the flow separates at 2/3 of L leaving an afterbody exposed to pressure loading. For this case, not only is the separation shifted upstream but, in addition, temporary impingement of the shear layers occurs at the sides of the afterbody.

The effects mentioned above can be discussed by looking at the variations of the Strouhal number. As a reminder, the nondimensional Strouhal number can be interpreted as the ratio of two time scales: one imposed by the body oscillation, $1/f_e$, and the other by the freestream velocity and the body geometry, D/V. Figure 2 gives an overview on the variations of Strouhal number in the different regimes classified as LEVS, ILEV, and TEVS as a function of the elongation ratio L/D. This graph is redrawn after presentations published by Naudascher & Wang (1993), Thang &

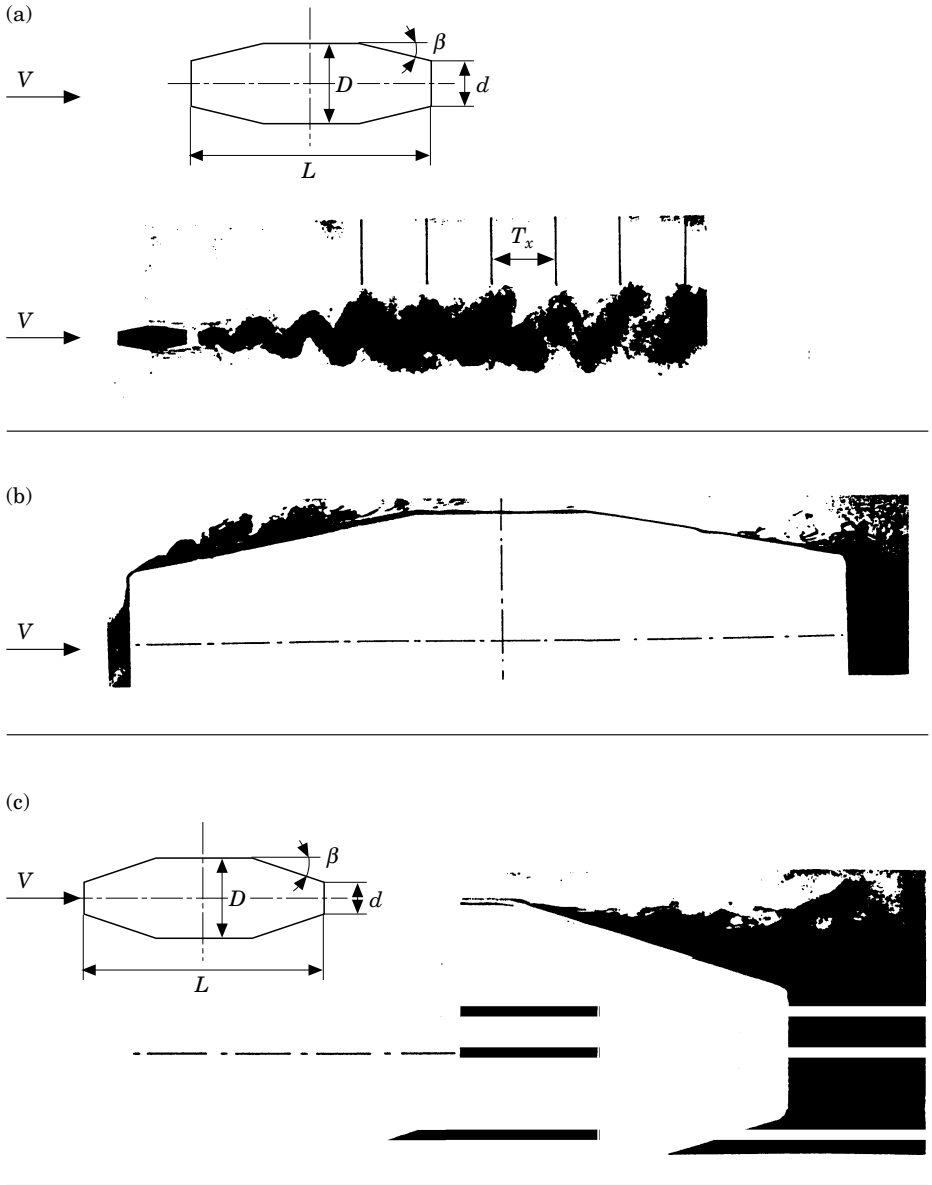

Figure 1. Visualization of flow separation from a cylinder of octagonal cross-section (Chaix 1972): (a) development of the Kármán vortex street in the wake for $\beta = 10°$, $d/D = 0{\cdot}6$, $D/L = 0{\cdot}33$, $\alpha = 0°$, $\mathrm{Re} = 3{\cdot}7 \times 10^4$, $S_o^{ne} = 0{\cdot}18$; (b) flow separation at the leading-edge and at the trailing-edge; (c) upstream shifting of the points of separation by increasing the wedge angle β, for $\beta = 16°$, $d/D = 0{\cdot}4$, $D/L = 0{\cdot}33$, $\alpha = 0°$, $\mathrm{Re} = 3{\cdot}7 \times 10^4$.

Naudascher (1991) and Knisely (1990). The data included were collected from experiments with non-oscillating profiles of various cross-sections at mostly low turbulence levels. It is reported by Nakamura & Yoshimura (1982) that the ILEV-excitation is especially sensitive to turbulence intensity. Turbulence can strongly influence the locations of separation and reattachment as well the development of the separated shear layers. Detailed studies of ILEV-excitation were described by

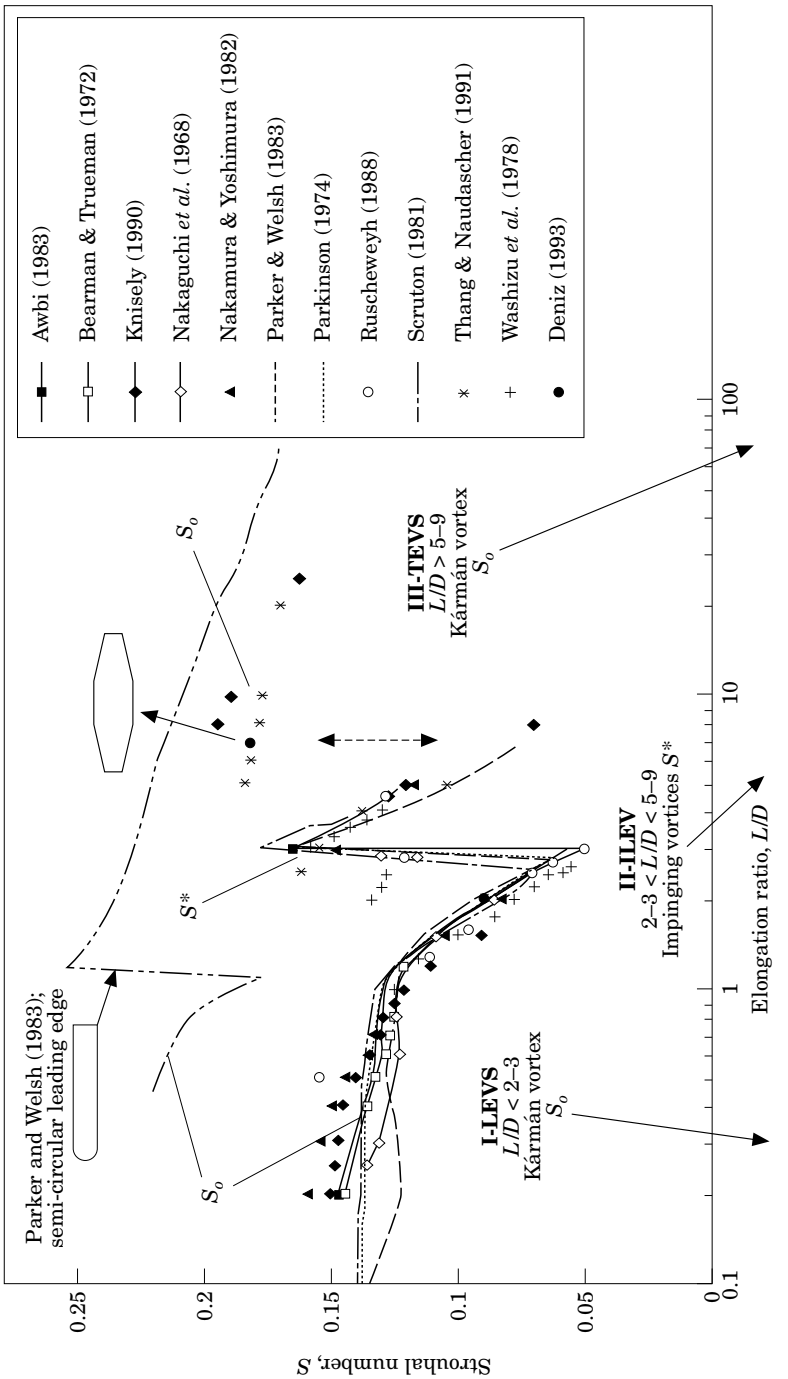

Figure 2. Classes of vortex formation observed with increasing elongation of different prismatic bodies: Class I leading-edge vortex shedding: Class II impringing leading-edge vortices; Class III trailing-edge vortex shedding.

Nakamura & Nakashima (1986) on the H-section profile which is particularly sensitive to this kind of excitation. Nakamura *et al.* (1991) found that the Strouhal number based on the side length L of a section is constant and equal to $0{\cdot}6n$, where n is an integer. An interesting feature is that ILEV is not affected by the presence of a splitter plate in the wake, while TEVS is largely suppressed—which is a way to distinguish the two phenomena.

Figure 2 shows the remarkable jumps and the double frequencies occurring with elongation ratios of $L/D \approx 2$–3 and $L/D \approx 4$–7, which mark the limits between the three flow regimes. These jumps are caused by the transitions of the significant vortex formations from the leading-edge to the trailing-edge. For very large elongation ratios, the Strouhal number, defined in terms of the thickness D of the cross-section, decreases due to the growing boundary-layer thickness at the sides of the profile, which widen the wake.

Movement-induced excitation (MIE), in contrast to IIE, is inherently linked to body movements and disappears when the body is at rest. In the case of an initial displacement, an unsteady force is induced that alters the fluid forces on the body. If this alteration leads to negative damping or to a transfer of energy to the moving body, a self-excited body vibration is possible. The negative fluid dynamic damping can also considerably reduce the total damping available to the body or structure. The term of *galloping* is usually applied to the large-amplitude, low-frequency oscillation of this category. Any bluff profile that can gallop can also exhibit vortex-induced vibrations (IIE), since an appreciable afterbody is a requirement for both. Characteristic of profiles sensitive to galloping are the negative lift-curve slopes as first described by Den Hartog (1934). Quasi-steady considerations [e.g., Parkinson (1974)] at very low frequencies of oscillation lead to fluid forces acting in phase with the instantaneous oscillation velocity.

The excitation mechanisms that will be considered in this paper are of type MIE and IIE. The goal is to provide insight into the interaction mechanisms of movement-induced and instability-induced excitation. Two different prismatic bodies are the objects under examination: a rectangular profile with an elongation ratio $L/D = 2$, and an octagonal profile with $L/D = 3{\cdot}33$ (see Figure 3). These differently shaped profiles show opposite behavior with respect to MIE: the rectangular profile has a negative lift-curve slope and the octagonal profile has a positive slope. Chaix (1972) showed that certain sharp-edged prismatic profiles, such as profiles with 6, 8, or 12 edges may show unstable behavior. In terms of vortex formation type (IIE) the rectangular profile belongs to the class of ILEV, and the octagonal profile to TEVS for flow without incidence. Both profiles show AEVS for larger incidence angles.

Leading-edge vortex shedding is typically observed for the square section cylinder (see Figure 2). The dynamic behavior of LEVS-sensitive profiles has been investigated for example by Bearman *et al.* (1987), Bearman & Luo (1988), Nakamura & Mizota (1975) and Nakamura & Matsukawa (1987).

2. EXPERIMENTS

Because of the complexity of flow-induced vibrations, one has to focus on selected phenomena in experimental studies. A high degree of simplification is needed in order to reduce the number of parameters influencing the results. In the present study, the following simplifications were employed. The oncoming flow was uniform and free of turbulence, which is characteristic of the towing tank experiments. The geometry employed in the present study involved two generic configurations, both being

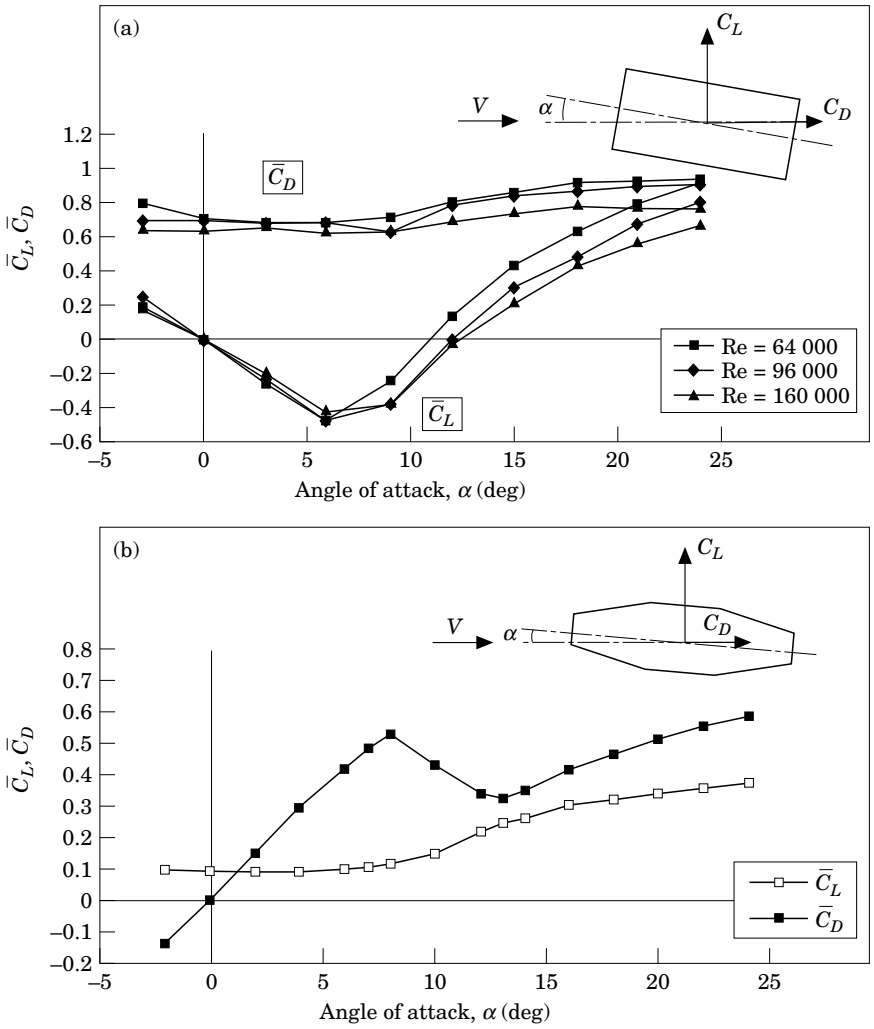

Figure 3. Time-mean life coefficient, $\bar{C}_L$, and drag coefficient, $\bar{C}_D$, of the non-oscillating (a) rectangular profile and (b) octagonal profile for varying angle of attack α and Reynolds numbers; for $\hat{\eta} = 0$, $S_e = 0$.

prismatic bodies with constant cross-section: (a) a rectangular profile with cross-sectional dimensions $D = 0{\cdot}03$ m and $L = 0{\cdot}06$ m; (b) an octagonal profile with dimensions $D = 0{\cdot}03$, $d = 0{\cdot}015$ m, $\beta = 12°$, and $L = 0{\cdot}1$ m (see Figure 1 for definitions of these parameters). For both of these body configurations, the spanwise dimension was 0·75 m. Moreover, the surfaces of these bodies were hydraulically smooth, and the corners had sharp edges. In order to minimize end effects, end-plates were employed. Both bodies were subjected to sinusoidal forcing in the direction transverse to the oncoming flow for two values of incidence angle: $\alpha = 0°$ and 10°.

The parameters used to define the experiment are the angle of attack α, the Reynolds number $\mathrm{Re} = VL/\nu$, the Strouhal number $S_e = f_d D/V$, and the dimensionless amplitude of oscillation $\hat{\eta} = \hat{y}/D$, in which V is the velocity of the oncoming flow.

In order to characterize the instantaneous flow patterns in relation to the loading on the bodies, the flow was visualized using the hydrogen bubble technique. A platinum wire of diameter 0·025 mm was used to generate pulsed timeline markets, which were

illuminated with stroboscopes. Images of these timeline patterns were recorded on a video system. The camera head of the video was located under water. Force measurements were undertaken using six piezoelectric transducers mounted within the two end-plates. The force coefficients were evaluated in the frequency domain, and the phase shifts were determined using cross-spectra of the measured forces and the motion of the body. Further details of the experimental set-up and the evaluation techniques are given by Staubli (1983) and Deniz (1993).

At this point, some definitions will be made. First, the lift and drag coefficients are defined by

$$C_L(t) = \frac{F_L(t)}{\frac{1}{2}\rho V^2 A}, \qquad C_D(t) = \frac{F_D(t)}{\frac{1}{2}\rho V^2 A}, \tag{1}$$

respectively.

The harmonic motion of the body is

$$\eta(t) = \hat{\eta}\cos(\omega_e t), \tag{2}$$

where $\hat{\eta}$ = amplitude of oscillation/D, and ω_e = angular frequency of the forced oscillation.

Analysis of the frequency components contributing to the lift force shows that basically four contributions are found:

$$\begin{aligned} C_L(t) &= \bar{C}_L + C_{Le}(t) + C_{Lo}(t) + \text{stochastic contributions} \\ &= \bar{C}_L + \hat{C}_{Le}\cos(\omega_e t + \Theta) + \hat{C}_{Lo}\cos(\omega_o t) + \text{stoch. contr.}, \end{aligned} \tag{3}$$

with $C_{Le}(t)$ = lift force component at the excitation frequency, $C_{Lo}(t)$ = lift force component at the frequency of instability-induced wake formation, Θ = phase shift between the lift component $C_{Le}(t)$ and the motion $\eta(t)$, and ω_o = angular frequency of the lift component $C_{Lo}(t)$; for the lift coefficient C_{Lo} no phase angle is defined. The spectral components $C_{Le}(t)$ and $C_{Lo}(t)$ were determined from spectral density distributions. The phase was Θ determined from cross-spectral density distributions of the motion $\eta(t)$ and lift force component $C_{Le}(t)$. The phase Θ determines whether there is an energy transfer from the fluid to the body or the opposite:

$$\begin{aligned} &0^\circ < \Theta < 180^\circ \qquad \text{energy transfer profile} \rightarrow \text{fluid} \\ &0^\circ > \Theta > 180^\circ \qquad \text{energy transfer fluid} \rightarrow \text{profile} \end{aligned} \tag{4}$$

Four different Strouhal numbers are defined:

$$S_e = \frac{f_e D}{V}, \quad S^* = \frac{f^* D}{V}, \quad S_o = \frac{f_o D}{V}, \quad S_o^{ne} = \frac{f_o^{ne} D}{V}; \tag{5}$$

thus, corresponding to the frequencies involved, S_e is the nondimensional excitation frequency, S^* the nondimensional frequency of impinging vortices, S_o the nondimensional frequency of wake vortex formation, and S_o^{ne} the nondimensional frequency of Kármán vortex shedding (where *ne* denotes *n*o external *e*xcitation; i.e., a stationary profile.

Experimentally frequencies were determined by means of power spectral densities of the measured lift forces acting on the profiles.

3. MEASUREMENTS WITH NON-OSCILLATING PROFILES

The two investigated profiles—the rectangular and the octagonal—were selected for this investigation because they show opposite lift characteristics. While there is an increasingly negative lift force for angles of attack up to 6° in case of the rectangular profile [Figure 3(a)], the lift is positively growing up to about 8° for the octagonal

profile [Figure 3(b)]. A necessary criterion for stability with respect to MIE is, according to Den Hartog (1934),

$$\frac{dC_L}{d\alpha} + C_D > 0. \tag{6}$$

This criterion is fulfilled for the octagonal profile but not for the rectangular profile, opening up the possibility of MIE in the range of $-6° < \alpha < +6°$. To which frequencies the rectangular profile is susceptible to excitation will be discussed on the basis of the energy transfer from the fluid to the body in Figures 6 and 7.

The change of sign of the slope $dC_L/d\alpha$ of the rectangular profile at $\alpha \approx 6°$ [Figure 3(a)] is caused by the reattachment on the flow-facing side of the profile. For the octagonal profile the change of sign occurs at $\alpha \approx 8°$ [Figure 3(b)] and is caused by the upstream shifting of the separation from the trailing-edge on the flow opposite side with increasing angle of attack (see also Figure 4).

Figure 4 shows the development of the Strouhal number S_o^{ne} with increasing angle of attack α for the non-oscillating case. The rectangular profile [Figure 4(a)] shows for the transition from ILEV to AEVS a jump in frequency. A maximum of S_o^{ne} is found for about 9°. Larger incidence leads to continuous reduction of the vortex formation frequency. Due to the flow separation at sharp corners, no significant influence of Reynolds number is observed.

For the octagonal profile [Figure 4(b)] three typical ranges have to be distinguished. For small incidence, the Strouhal number of 0·18 is representative for TEVS as can be seen from comparison with Figure 2. For angles of attack $\alpha > 12°$ clearly defined AEVS occurs. For both profiles the decay of S_o^{ne} observed for large incidence can be explained by the increasing width of the wake, as demonstrated for example by Roshko (1954) and Knisely (1990). In an intermediate range $5° < \alpha < 12°$ [Figure 4(b)], no periodic force fluctuations could be evaluated for the octagonal profile.

Figure 5 displays magnitude spectra of the lift forces acting on the non-oscillating rectangular profile for different angles of attack. The spectra show the dominant peaks in the frequency domain associated with the wake vortes formation $S_o(\alpha < 6°)$ and AEVS ($\alpha > 6°$) and, at an incidence of $\alpha = 6°$, random or intermittent effects which are typical for the transition from one regime to another.

4. MEASUREMENTS WITH OSCILLATING PROFILES

The profiles were oscillated at a variable frequency, f_e, by means of a hydraulic actuator. The drive and the profile were stiff enough to avoid any feedback of the fluid forces on the motion of the body. Measurements with varying frequency were performed at three different amplitudes of oscillation. The wide range of frequency variation allowed investigation of the effects of MIE, IIE, and fluid dynamic mass. For the experiments with forced oscillation the Reynolds number was kept constant at $\mathrm{Re} = 10^5$. An increasing amplitude at a constant frequency corresponds to an increased maximum of the angle of attack $\hat{\alpha} = \arctan(2\pi\hat{\eta}S_e)$. At low frequencies, only in the case of zero angle of attack, a linear relationship of the lift force and amplitude may be expected, if the quasi-steady condition is fulfilled. At higher oscillation frequencies, where inertia effects dominate, the lift force will grow linearly with amplitude.

Figures 6(a) and 7(a) show the lift coefficients $\hat{C}_{Le}$ for the rectangular profile as a function of the nondimensional excitation frequency, S_e. Magnitudes increase with increasing frequencies for both cases, that is without ($\alpha = 0°$) and with incidence

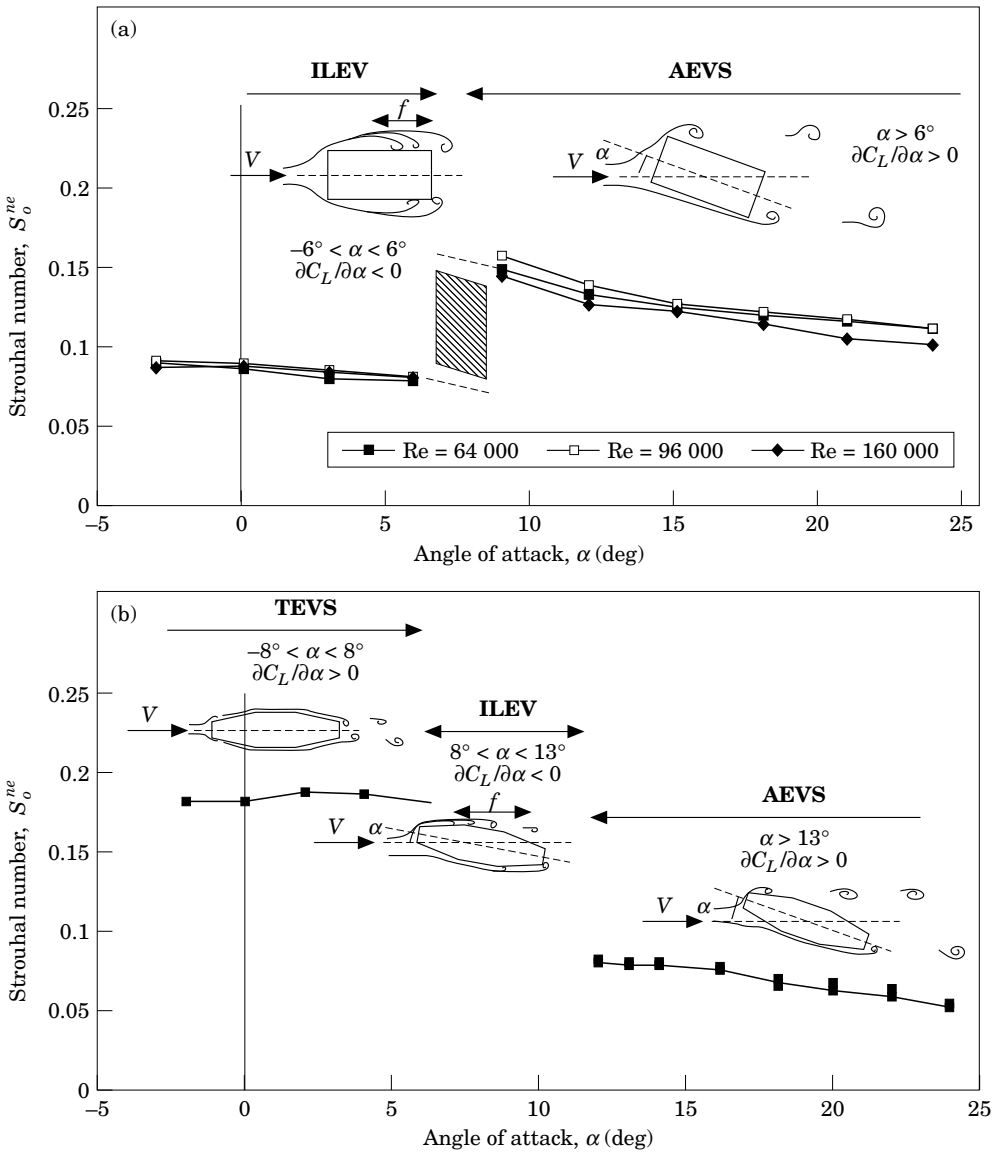

Figure 4. Variation of the Strouhal number for increasing angle of attack α for (a) the non-oscillating rectangular profile and (b) the octagonal profile; for $\hat{\eta} = 0$, $S_e = 0$.

($\alpha = 10°$) corresponding to different flow regimes, as can be seen in Figure 3. In Figures 6(a) an 7(a) a first, rather broad-banded, local maximum is found near the frequency S_o^{ne} where resonance with the instability-induced excitation occurs. For excitation frequencies above $S_e = 0{\cdot}15$, $\hat{C}_{Le}$ increases linearly with the amplitude $\hat{\eta}$ and proportional to the square of S_e according to the inertia effects of the surrounding fluid. The basic trends of the response characteristics of the cases with and without incidence are very much alike; at high excitation frequencies fluid inertia effects dominate the flow field. However, with respect to the possibility of fluid-elastic oscillations, the two cases differ considerably, as can be concluded from the phase angle between the lift force and the displacement.

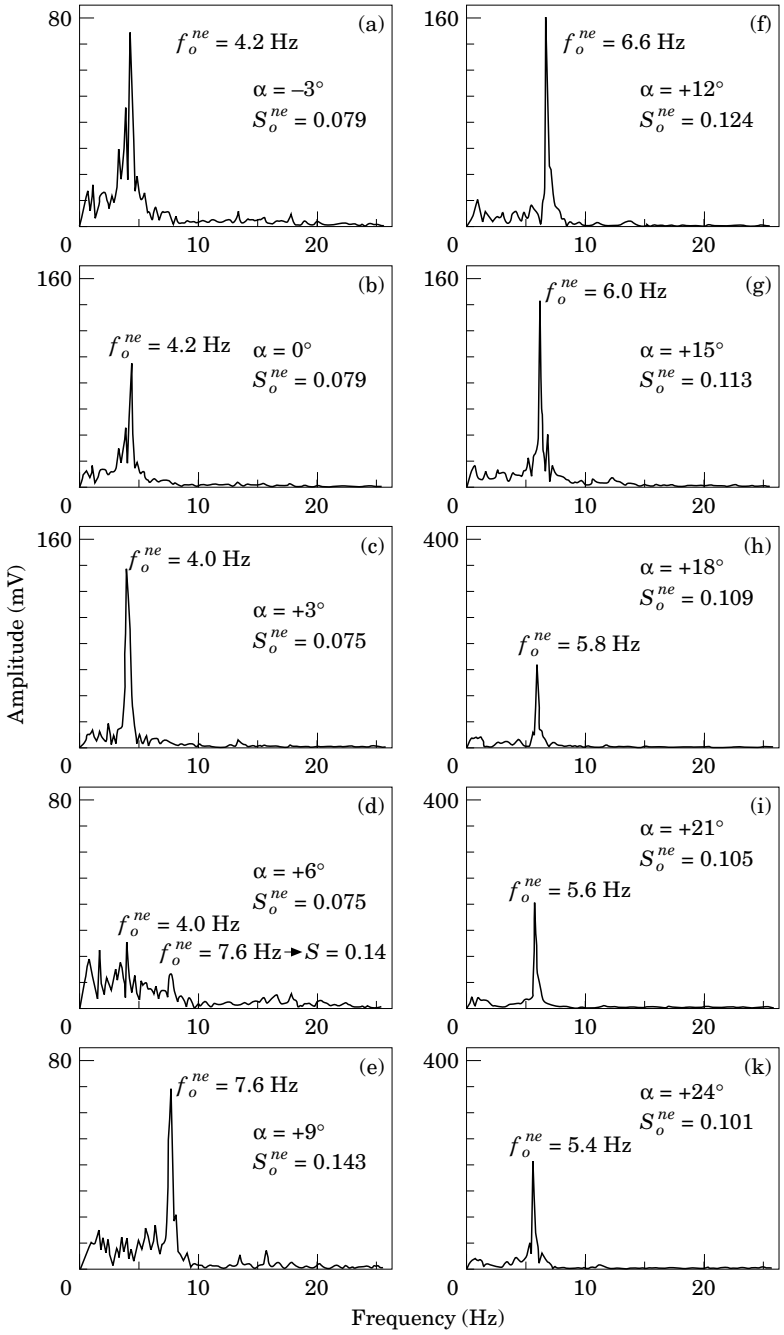

Figure 5. Magnitude spectra of the lift forces acting on the non-oscillating rectangular profile for increasing angle of attack α.

Figures 6(b) and 7(b) display the phase Θ for the cases without and with incidence of the rectangular profile. Phase angles above 360° at the lowest excitation frequencies in Figure 6(b) indicate an energy transfer from the fluid to the body, meaning that galloping oscillations of elastically mounted profiles could be excited. According to the phase angle in Figure 7(b) no such movement-induced excitation is possible for an

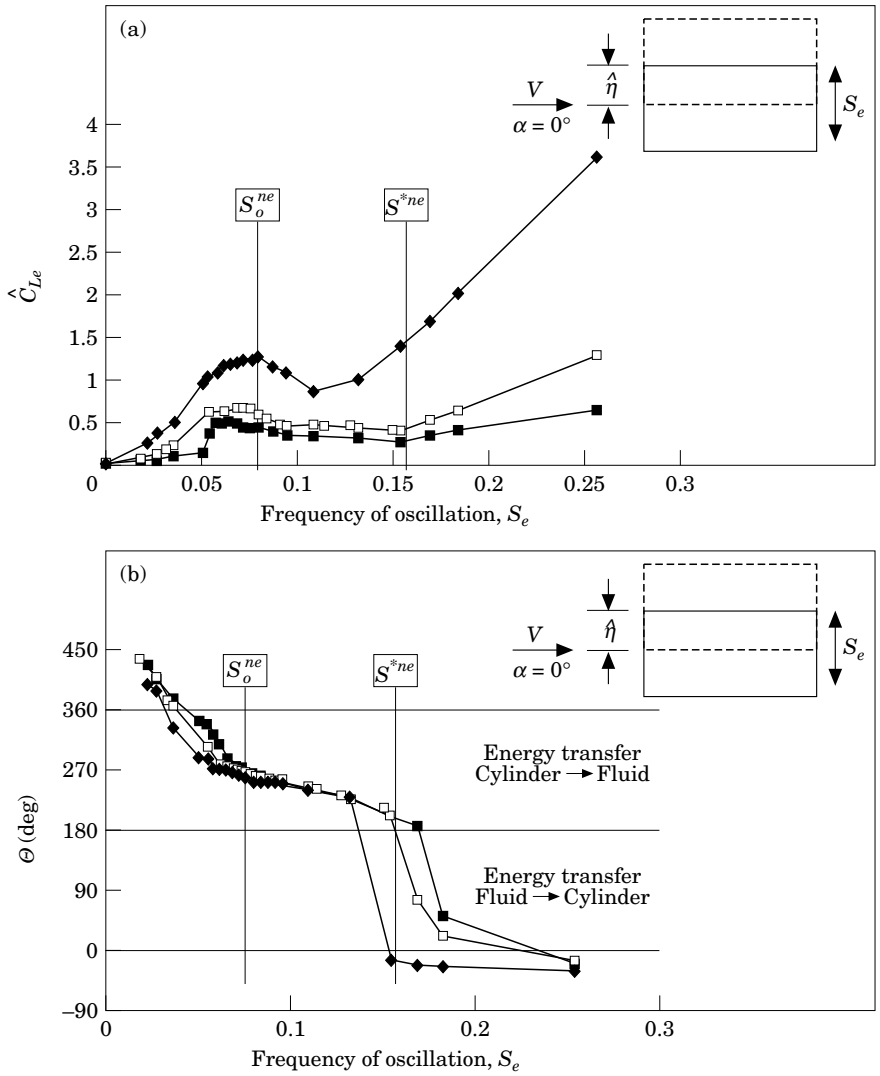

Figure 6. Response characteristics of the rectangular profile at an angle of attack $\alpha = 0°$ showing: (a) the externally excited life component $\hat{C}_{Le}$, and (b) the phase angle Θ between $C_{Le}(t)$ and the displacement $\eta(t)$. In all cases, Re = 10^5; —■—, $\hat{\eta} = 0{\cdot}05$; —□—, $\hat{\eta} = 0{\cdot}10$; —◆—, $\hat{\eta} = 0{\cdot}30$.

angle of attack of $\alpha = 10°$, confirming the Den Hartog criterion applied to the data of Figure 3(a).

At frequencies above the resonance observed for $\hat{C}_{Le}$, the phase angles Θ between the lift force and the displacement again pass a sector of possible fluid-elastic excitation with an energy transfer from the fluid to the body. This sector lies for $\alpha = 0°$ near $S_e = S^*$, and for $\alpha = 10°$ near $S_e = S_0$. The observed phase jump in this range is associated with a remarkable change of the vortex formation and its phasing with respect to the displacement, as will be shown in Section 5. This typical instability-induced excitation mechanism is observed irrespective of the incidence of the flow in a similar manner in Figures 6(b) and 7(b).

The fluid-dynamic response of the rectangular profile for $\alpha = 0°$ is dominated by the ILEV behavior [Figure 6(a, b)]. For $\alpha = 10°$ the AEVS controls the flow field.

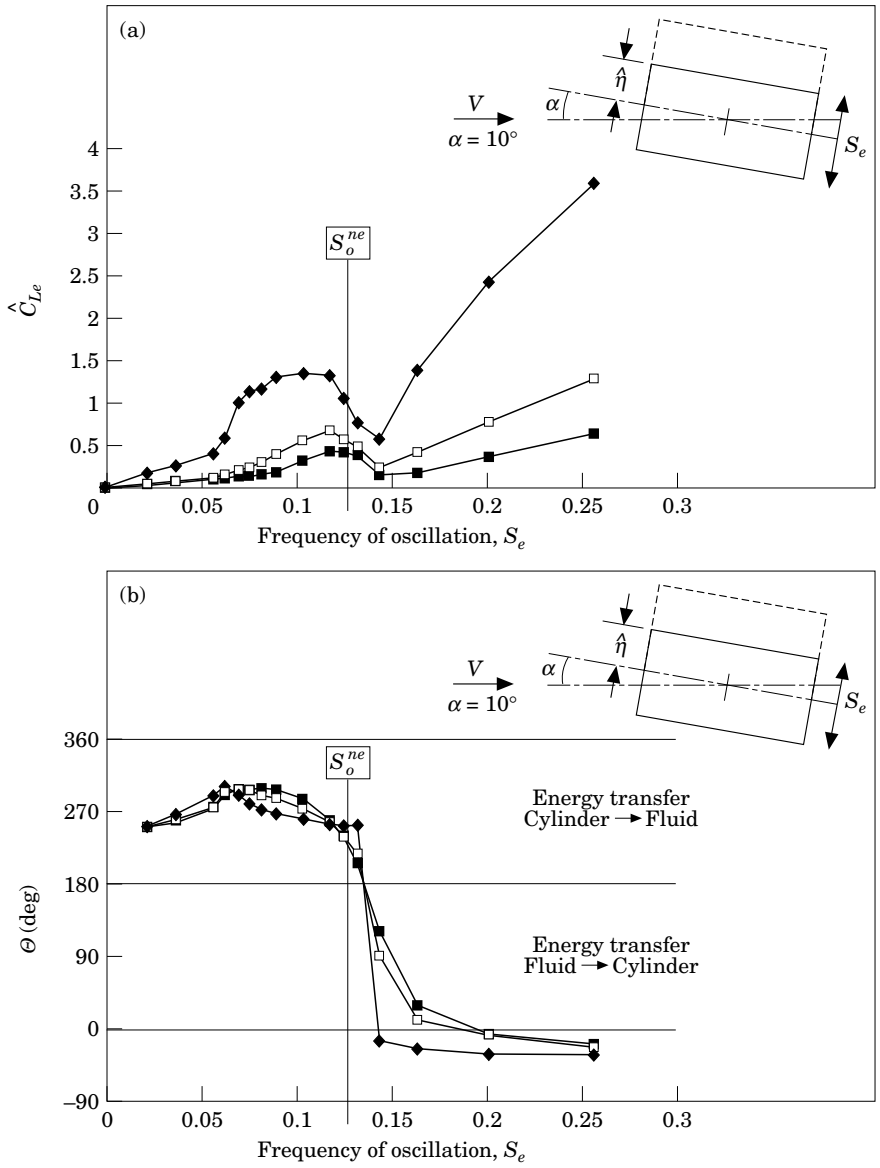

Figure 7. Response characteristics of the rectangular profile at an angle of attack $\alpha = 10°$ showing: (a) the externally excited lift component $\hat{C}_{Le}$; and (b) the phase angle Θ between $C_{Le}(t)$ and the displacement $\eta(t)$. In all cases, Re = 10^5; —■—, $\hat{\eta} = 0{\cdot}05$; —□—, $\hat{\eta} = 0{\cdot}10$; —◆—, $\hat{\eta} = 0{\cdot}30$.

The frequency where the phase jump occurs is influenced by the displacement amplitude. With increasing amplitude, the phase jump becomes slightly larger and steeper and is shifted towards lower frequencies.

Figures 8 and 9 show the response characteristics (lift and phase) of the octagonal profile with and without incidence. Almost no effects of resonance are detectable, either in an amplification of the lift coefficient or in a phase jump. The lift forces at the higher frequencies of oscillation are dominated by fluid inertia effects that are confirmed by the phase angles tending to a zero value. For very low frequencies of oscillation the phase Θ tends to $-90°$ indicating forces acting opposite to the

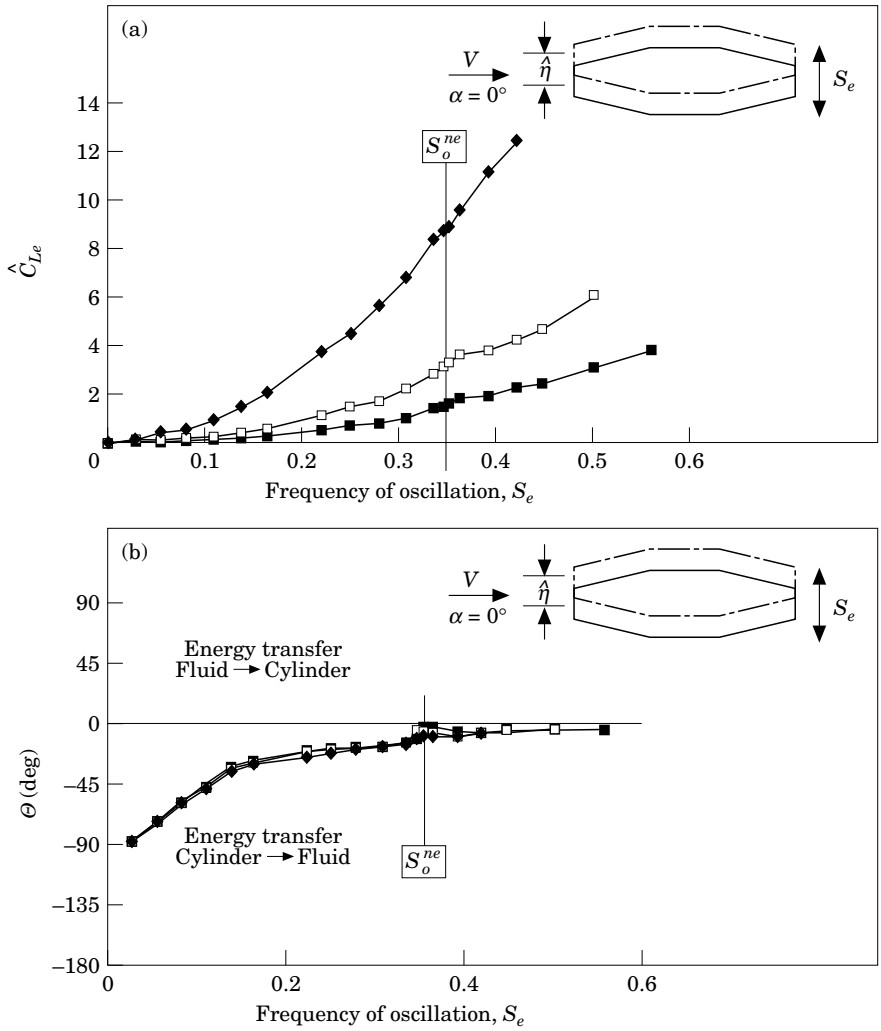

Figure 8. Response characteristics of the octagonal profile at an angle of attack $\alpha = 0°$ showing: (a) externally excited lift component $\hat{C}_{Le}$; and (b) the phase angle Θ between $C_{Le}(t)$ and the displacement $\eta(t)$. Re $= 10^5$; —■—, $\hat{\eta} = 0{\cdot}05$; —□—, $\hat{\eta} = 0{\cdot}10$; —◆—, $\hat{\eta} = 0{\cdot}30$.

oscillation velocity, which is equivalent to viscous damping, allowing quasi-steady modeling of the forces.

It is noted that the Strouhal number of the octagonal profile is defined with its thickness D and not with the thickness d of the trailing-end. Using the trailing-end thickness, $d = 2D$, would lead to a Strouhal number of trailing-edge vortex shedding of the non-oscillating body of $S^{ne}_{od} = 0{\cdot}18$ instead of $S^{ne}_{oD} = 0{\cdot}36$.

5. FLOW VISUALIZATION

Flow visualization is a valuable tool for interpretation of the interactions of the flow structures with an oscillating body and to clarify the fluid dynamic effects leading to the measured response characteristics. In the following sequences of pictures taken with the rectangular profile (angle of attack $\alpha = 0°$) oscillating at a constant displacement amplitude of $\hat{\eta} = 0{\cdot}1$ will be discussed. Frequencies were varied in the range of $S_e = 0$

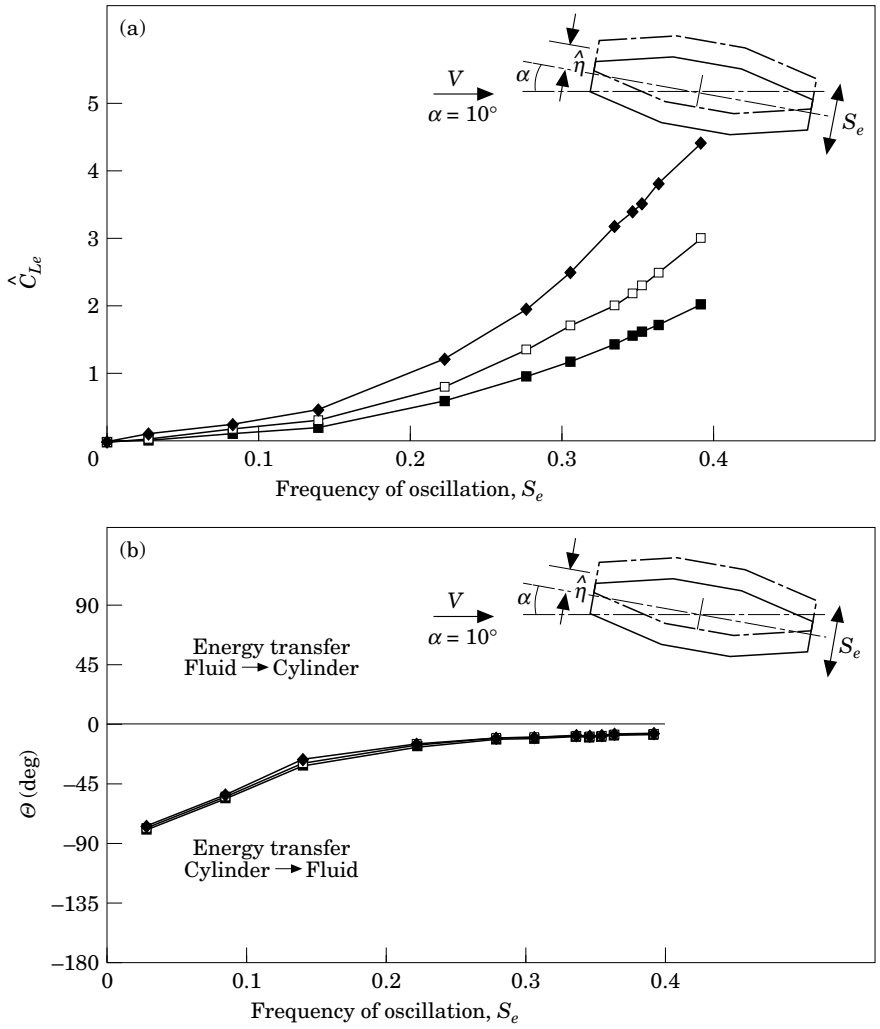

Figure 9. Response characteristics of the octagonal profile at an angle of attack $\alpha = 10°$ showing: (a) externally excited lift component $\hat{C}_{Le}$; and (b) the phase angle Θ between $C_{Le}(t)$ and the displacement $\eta(t)$. $\mathrm{Re} = 10^5$; —■—, $\hat{\eta} = 0{\cdot}05$; —□—, $\hat{\eta} = 0{\cdot}07$; —◆—, $\hat{\eta} = 0{\cdot}10$.

to 1. In order to obtain better picture quality, the Reynolds number was lowered for visualization by a factor of 10.

A general feature of the flow patterns is the superpositon of a series of phenomena. The separation at the leading-edge produces unstable shear-layers, leading to small-scale Bloor–Gerrard vortices (Bloor 1964; Gerrard 1966). In the far wake behind the profile, the shear-layers reorganize to the von Kármán vortex street at the nondimensional frequency S_o. Small-scale vortices convecting on the surfaces and vortices in the far wake will have practically no influence on forces acting upon the non-oscillating rectangular profile. The first effect will cancel, due to the occurrence of a series of counteracting vortices, and the second induces only very small pressure loading on the body, due to the distance of the vortex formation from the body. The shear layers separated from the leading edges impinge at a frequency S^* alternately on the upper and lower surfaces and play an essential role in case of the rectangular profile with $L/D = 2$.

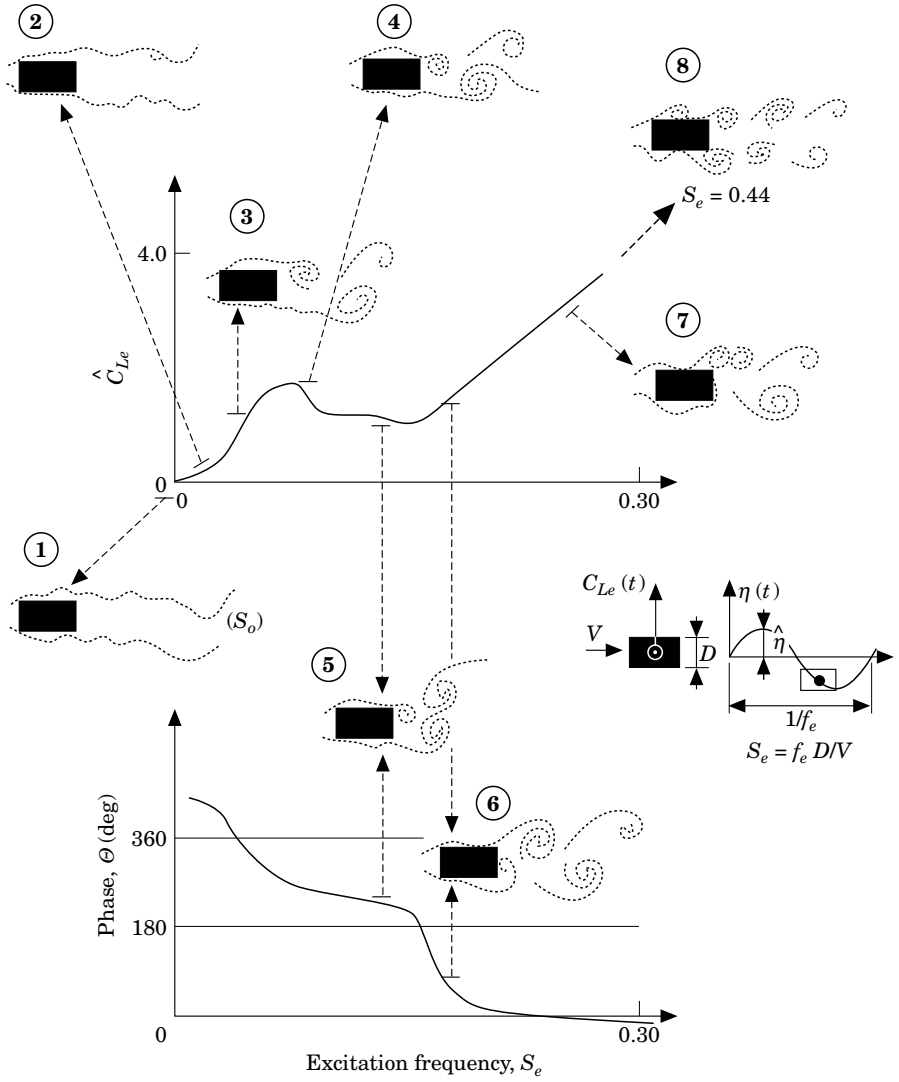

Figure 10. Overview of typical flow structures observed around the rectangular profile in relation to amplitude and phase of the measured lift forces; $\alpha = 0°$, $\hat{\eta} = 0{\cdot}10$; $\mathrm{Re}_{\mathrm{visual}} \simeq 10^4$, $\mathrm{Re}_{\mathrm{meas}} \simeq 10^5$.

If the body starts to oscillate, all of the above-mentioned effects are altered and when there is coincidence of the excitation frequency S_e with one of the instabilities, vortex intensities are amplified and pressure loadings eventually increase.

Figure 10 gives an overview of typical vortex formation in relation to the response characteristics of the lift force. Data are equivalent to those displayed in Figure 6. The sketches of vortices are drawn after video recordings and show schematically the dominant effects. In Figures 11(a) to 11(c) additional information on variations of the flow patterns with increasing oscillation frequency is given by means of views at the upper surface and at the wake for two instants during one cycle of oscillation. The pictures showing the flow field above the upper surface are taken with a platinum wire just upstream of the profile, while for pictures of the wake, a wire was mounted right behind the trailing end. Time sequences of development in the wake as a function of oscillation frequency are displayed in Figure 12. These picture series allow us to observe

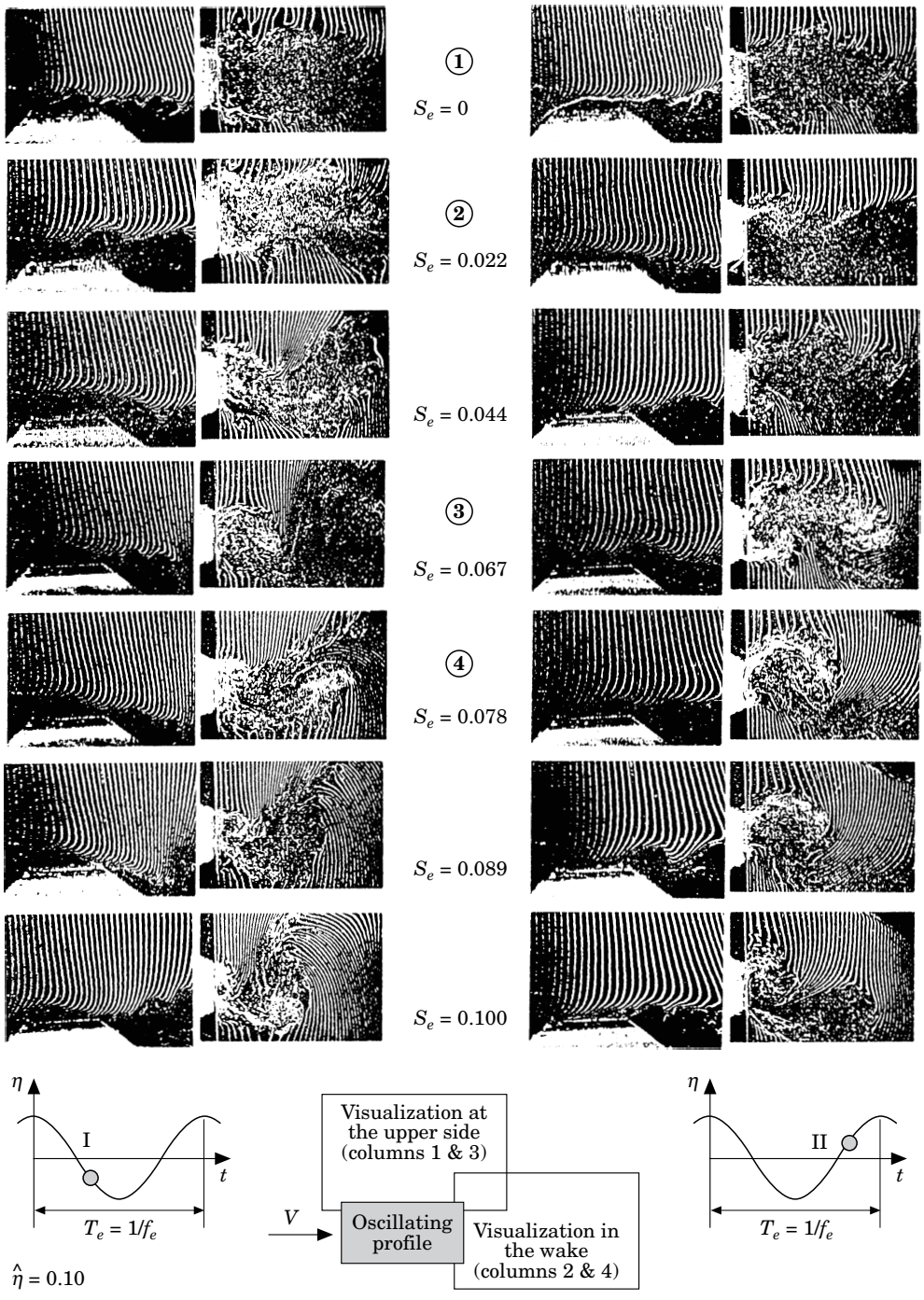

Figure 11. Changes of the flow structure for increasing frequency of oscillation S_e for two positions (I and II) during one cycle of oscillation. Pictures taken on the upper surface with a platinum wire upstream of the leading-edge (columns 1 and 3) and pictures of the wake taken with a platinum wire behind the trailing-end (columns 2 and 4); $\mathrm{Re} \simeq 10^4$.

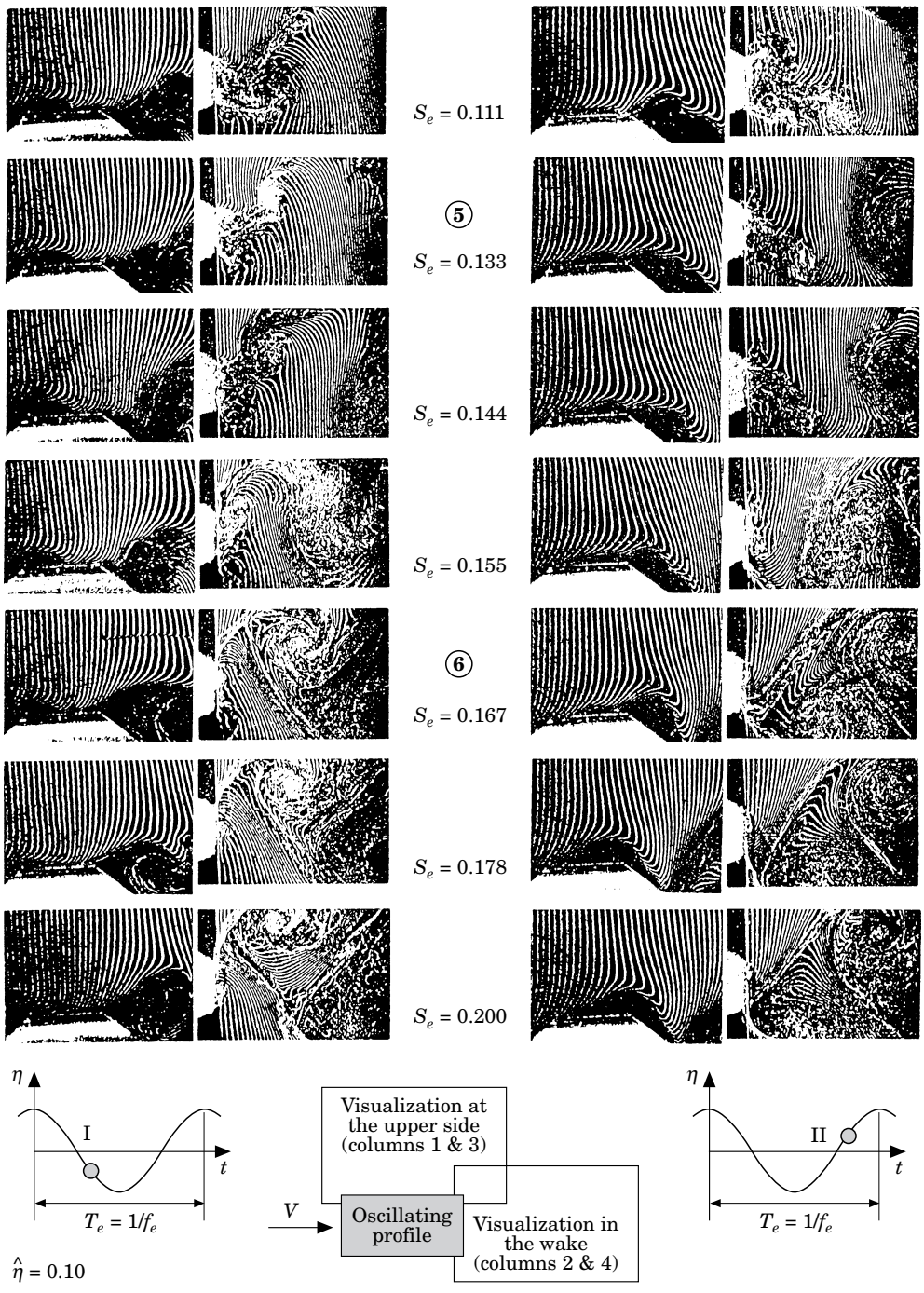

Figure 11. Continued.

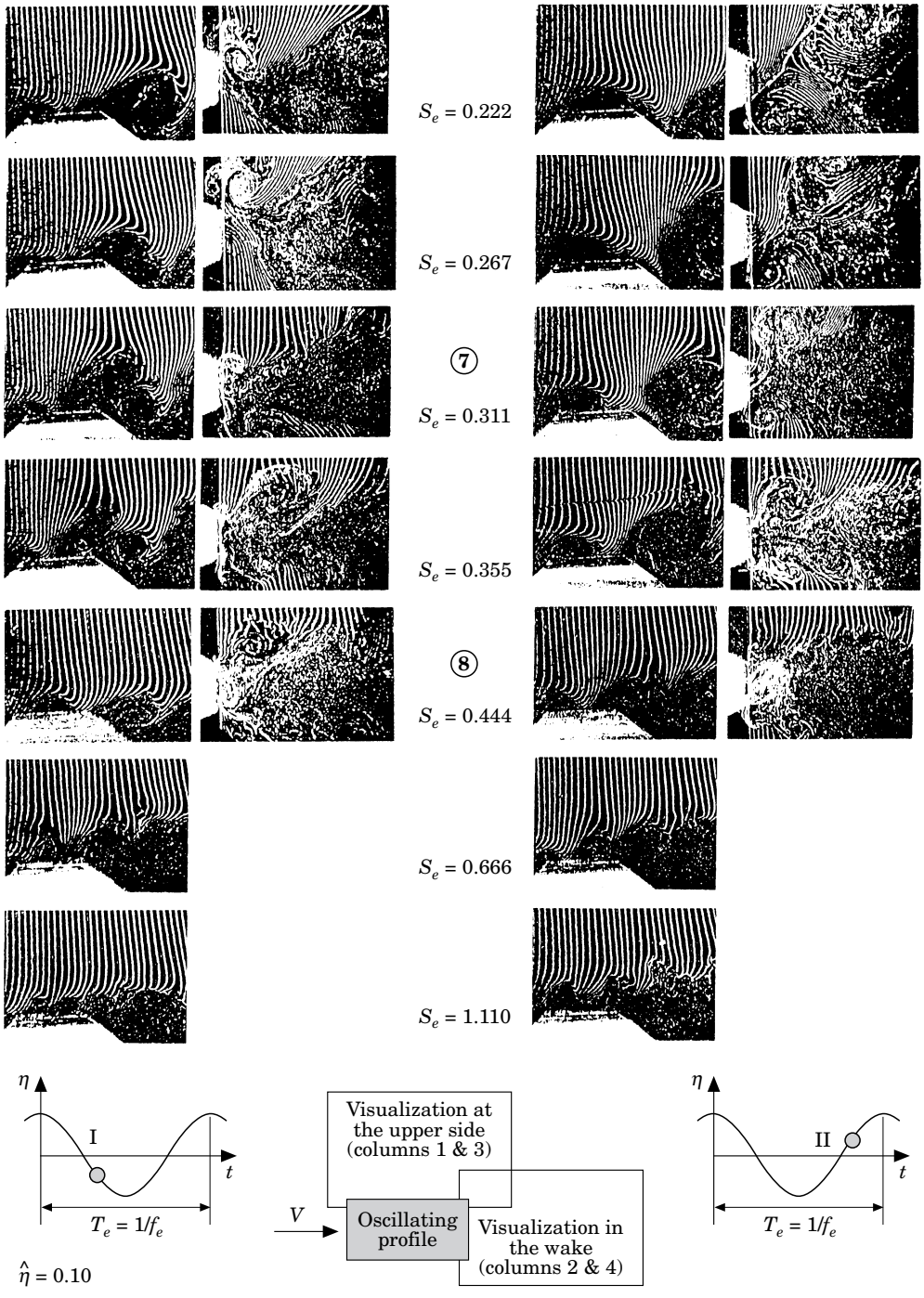

Figure 11. Continued.

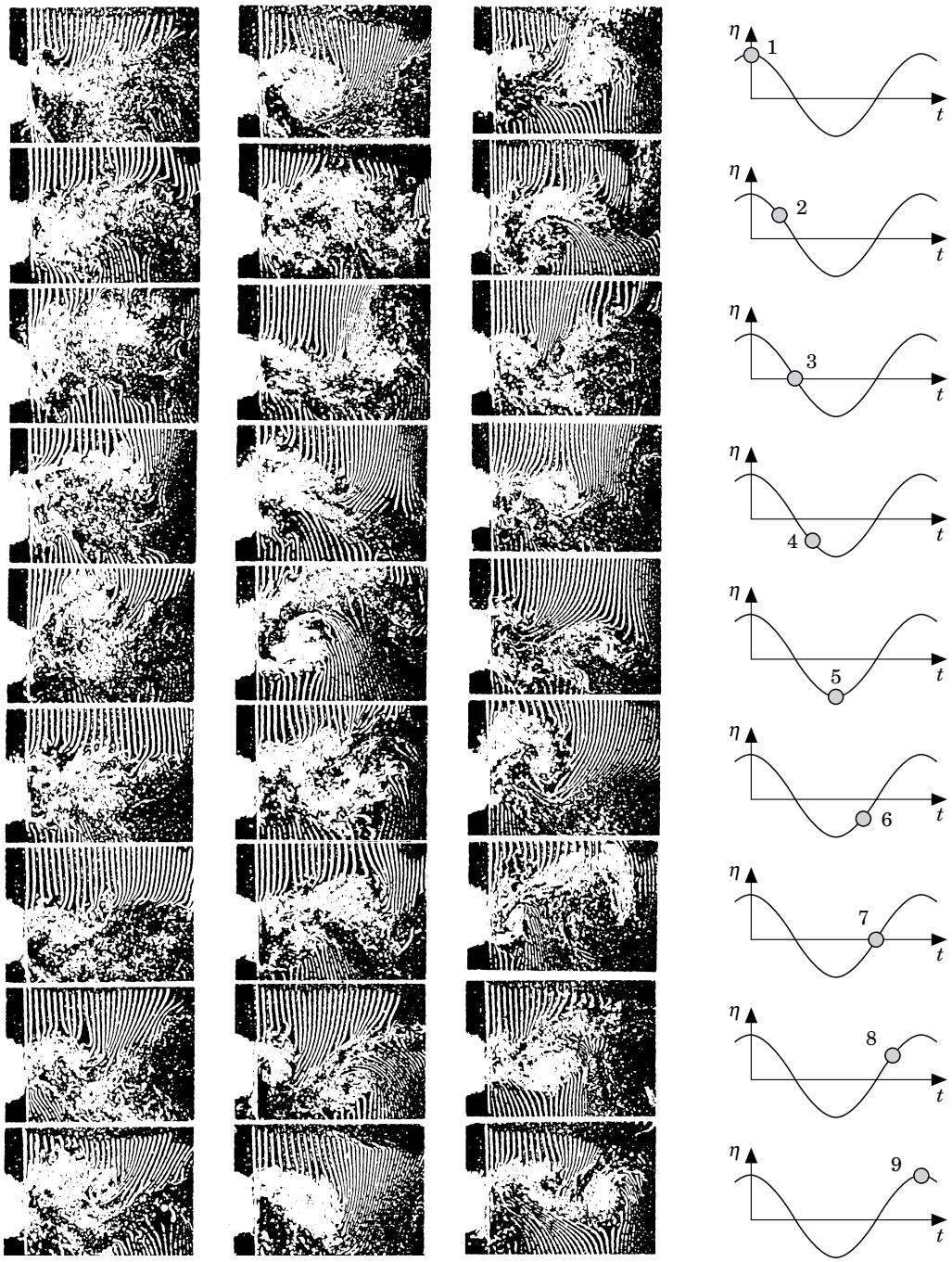

Figure 12. Time sequences of the flow structure in the wake of the rectangular profile for increasing frequency of oscillation S_e. The vertical columns show nine frames during one cycle of oscillation, with the first and the last in upmost position; $\hat{\eta} = 0{\cdot}10$; $\mathrm{Re} \simeq 10^4$.

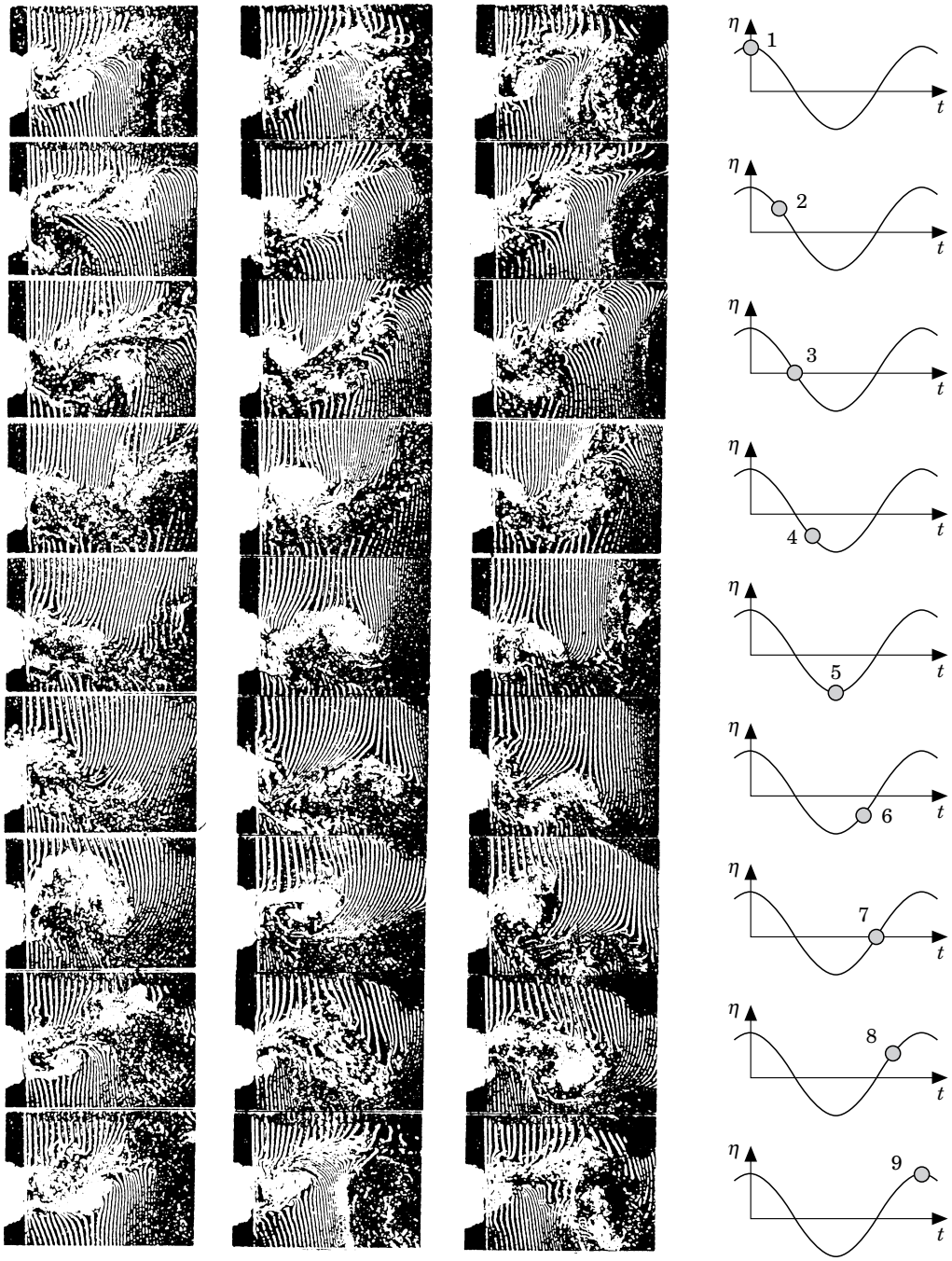

Figure 12. Continued.

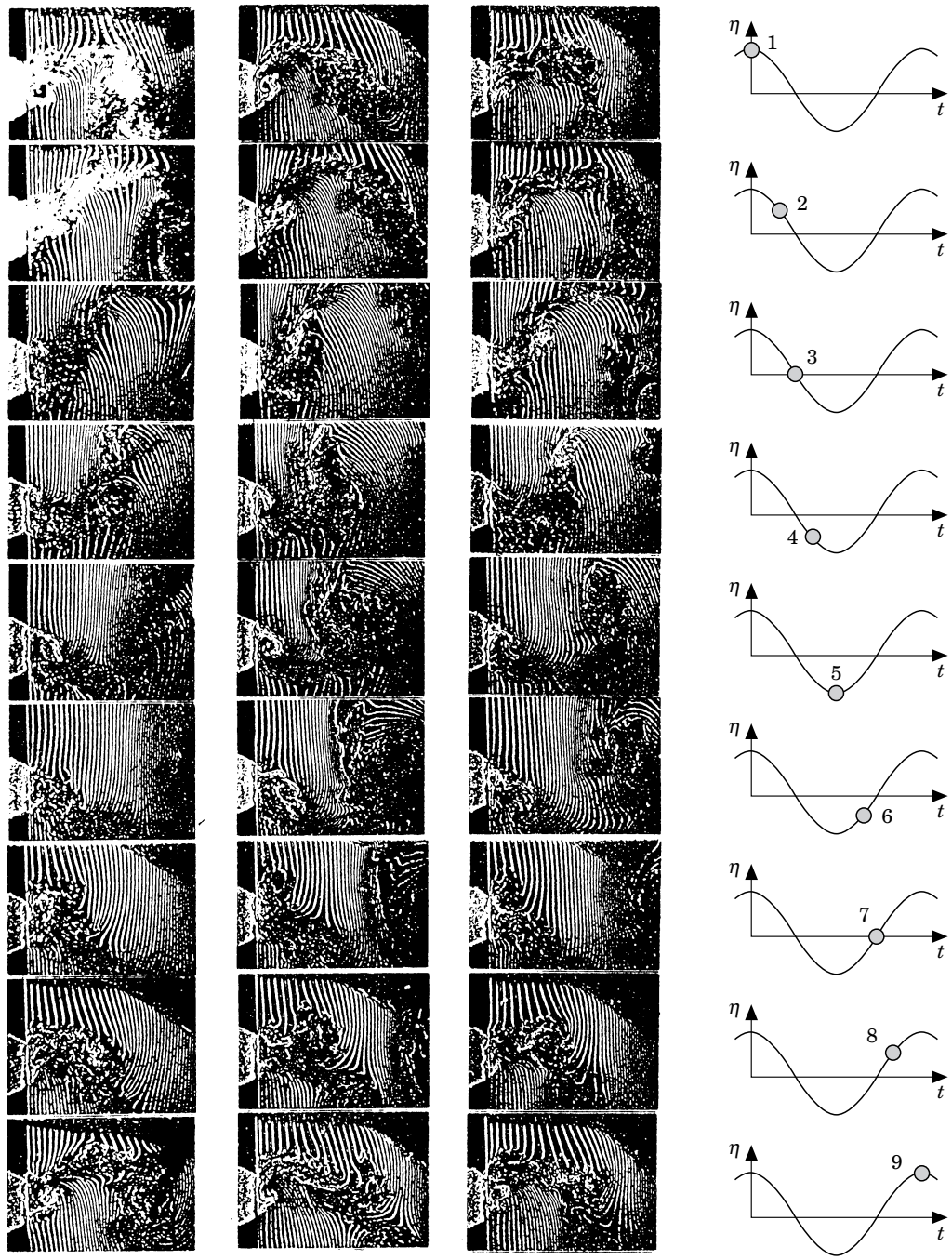

Figure 12. Continued.

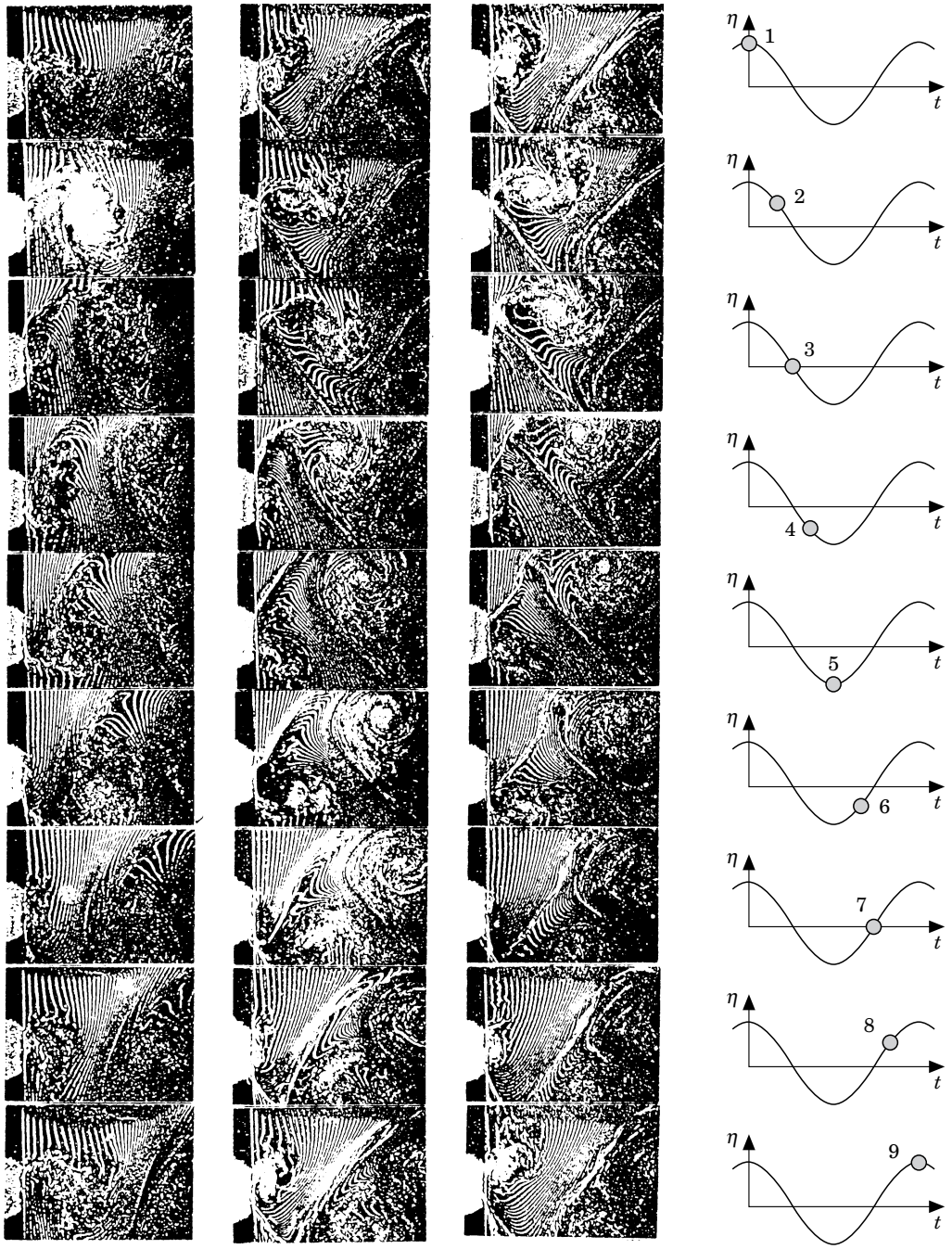

Figure 12. Continued.

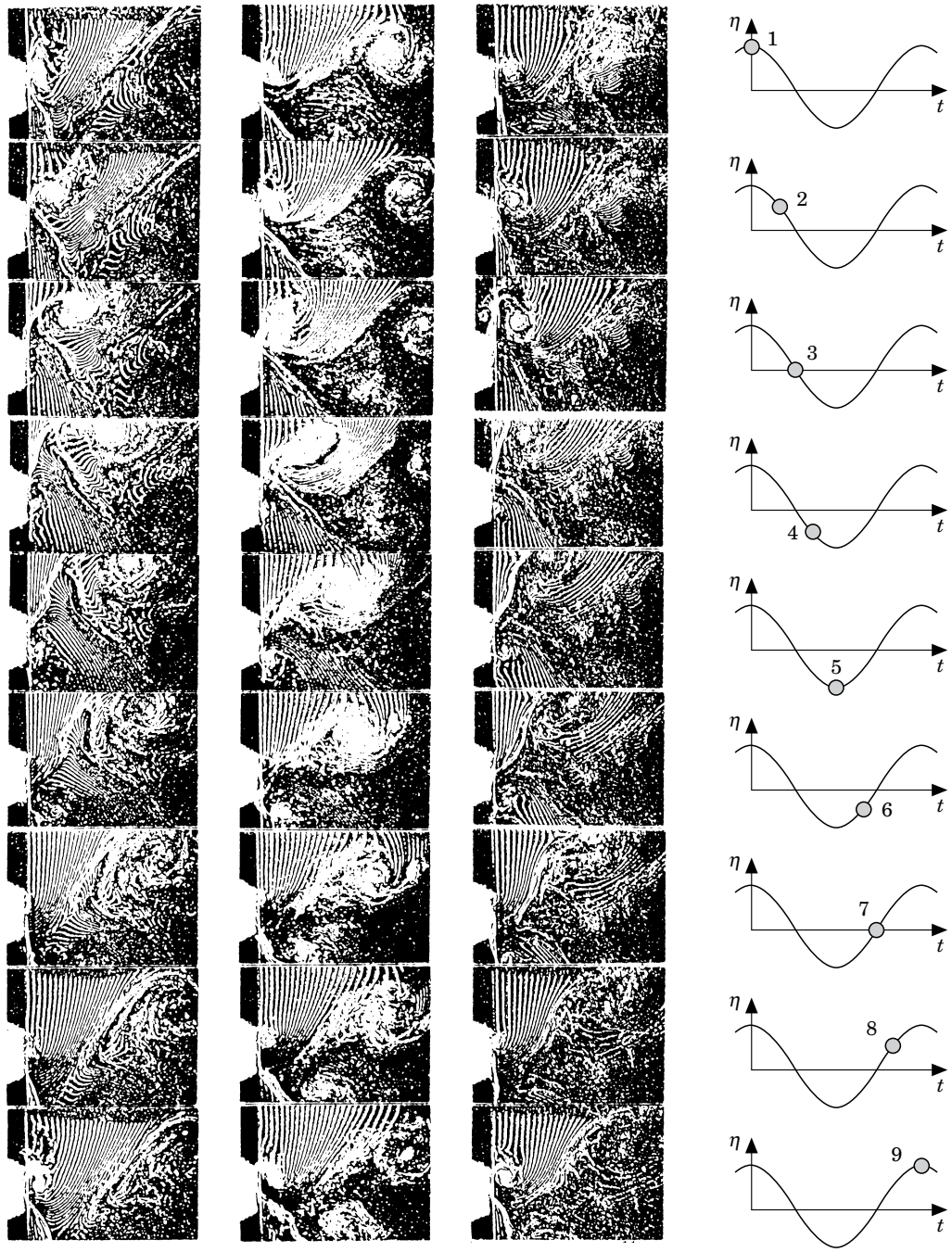

Figure 12. Continued.

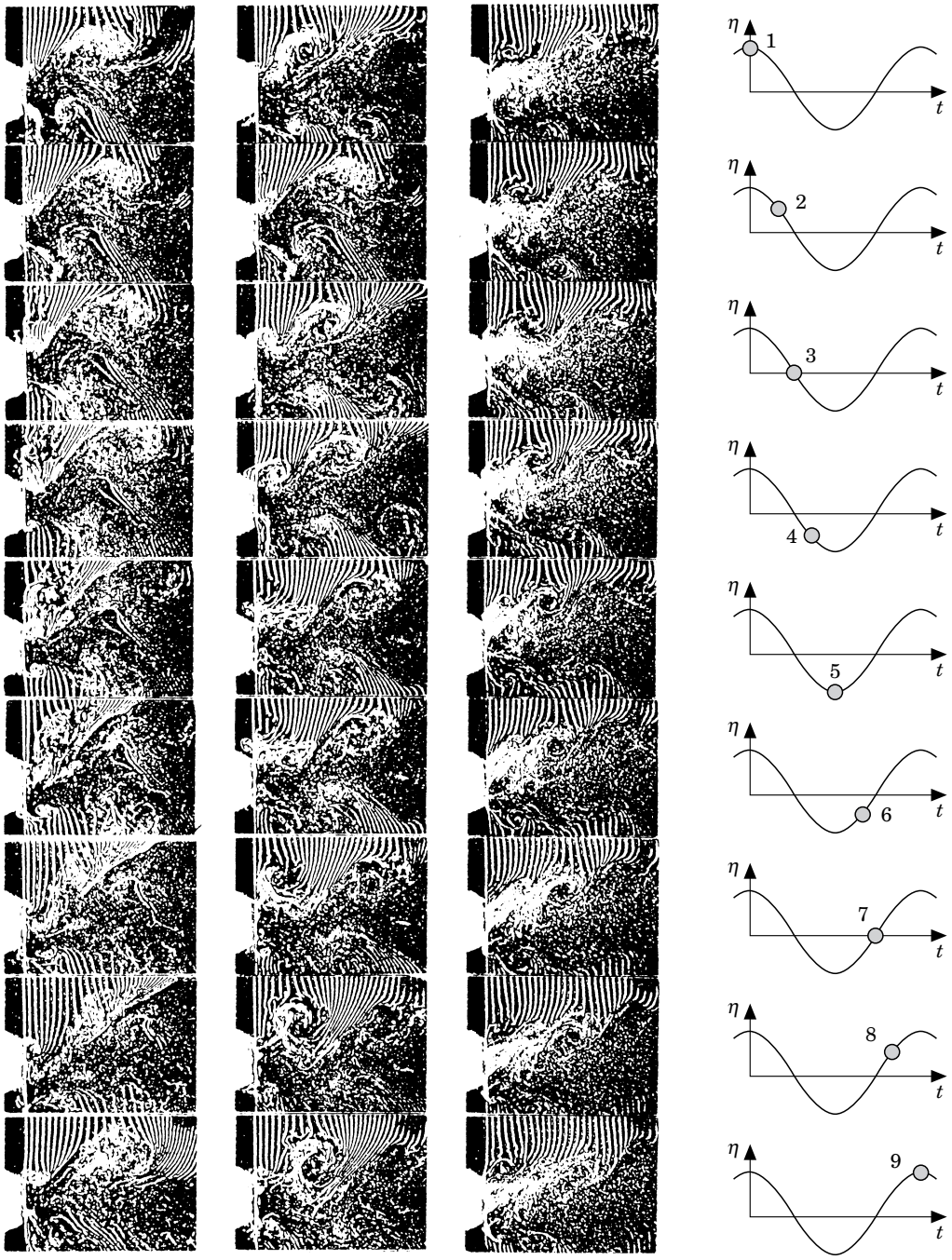

Figure 12. Continued.

the vortex formation in more detail, since one cycle of body oscillation is resolved with eight frames, and a ninth is showing the degree of periodicity of the vortical structures.

Point ① characterizes the non-oscillating case. The flow separates at the leading-edge and no reattachment occurs. The separated shear-layers show the distinct formation of Bloor-Gerrard vortices convecting into the wake. The formation region of the wake vortices (Kármán vortices) behind the trailing-edge is large and cannot be detected in the close-up view of the wake displayed in Figures 11 and 12.

Point ②, at very low oscillation frequency, corresponds to a range of frequencies where quasi-steady considerations are valid, that is, that the flow fields and forces are equal to the stationary case with small incidence (e.g., for $S_e = 0{\cdot}022$, $\hat{\alpha} = 0{\cdot}8°$). It is for these low frequencies that the rectangular profile tends to be sensitive to movement-induced galloping oscillations. The time sequence displayed in Figure 12 demonstrates that the body oscillation does not force periodicity in the wake flow field for this very low oscillation frequency.

With increased oscillation frequency the formation region of wake vortices becomes shorter and the organization of the vortices is enhanced. Point ③ lies at the beginning of the range with amplified lift coefficients. The frequency $S_e = 0{\cdot}078$ of point ④ is identical to the frequency of the Kármán vortex shedding of the non-oscillating rectangular profile $S_o^{ne} = 0{\cdot}078$. Here, the vortex formation synchronizes with the body motion and the vortex formation is intensified, as can be seen from the time sequence of Figure 12. With increasing frequency of oscillation, the vortex formation region in the wake is reduced in length.

Major changes with respect to the alternating vortex formation in the wake occur in the flow field visualized in point ⑤. Movement-induced vortices at the leading edge and vortices forming at the trailing edge coalesce behind the trailing edge and form large vortices in the far wake. These coalescing vortices have the same sense of rotation; however, since on the opposite side counter-rotating vortices form, there is a certain annihilation of induced forces at the oscillation frequency. This effect is shown in Figure 6(a) as a locally attenuated increase of the lift coefficient C_{Le}. A further observation is that the location of reattachment of the leading-edge vortices is shifted upstream with increasing frequency.

The frequency of point ⑥ lies close to the frequency S^* of the impinging vortices observed for the non-oscillating profile. Accordingly, the vortex separating from the leading-edge is enhanced. Again there is always coalescence of two vortices of the same sense of rotating behind the trailing-edge; however, this time there is a marked change in the phasing of the formation of the large wake vortices relative to the movement. This phasing reflects the phase jump observed in the lift forces and affects fluid forces which cause a positive energy transfer from the fluid to the body. A vortex street with well defined large vortices is completely synchronized with the movement of the profile and the induced oscillations of the near wake (see Figure 12). It is in this range of excitation frequencies that the magnitudes of the lift coefficient $\hat{C}_{Le}$ start to rise again.

In point ⑦ important modulations of the wake vortex formation can be observed. In this case leading-edge vortices convect downstream and interact with vortices formed behind the trailing edge; however, no periodic coalescence or pairing occurs immediately at the trailing-edge. An interesting feature of this frequency is that the convection time of the leading-edge vortices, $T_{conv} = L/V_{conv} \approx L/0{\cdot}6V$, corresponds approximately to the period of oscillation $T_{conv} \approx T_e = 1/f_e$, assuming an average convection velocity of $0{\cdot}6$ times the approach velocity V.

Point ⑧ relates to an oscillation frequency where fluid inertia dominates the forces. The frequency of oscillation is five times higher than that of the Kármán vortex street.

For each cycle of oscillation small-scale vortices form at the leading-edge and propagate along the surfaces downstream. In the wake there is no discernible interaction of these vortices from the lower and upper layers. Between the upper and lower vortex layer the fluid remains almost at rest. The structure of the wake is comparable to that of point ①, with the wake of the non-oscillating profile. As the time sequence of Figure 12 shows one cycle of the body oscillation, variations due to the Kármán street are not discernible, since its period is five times larger.

6. CONCLUSIONS

The forces acting upon prismatic bodies are directly related to the flow structure and the formation of vortices at the leading and trailing edge. These vortices strongly interact with each other as well as with the body surfaces. All effects are very sensitive to the geometrical variation such as the elongation ratio of the rectangular profile or the machining of leading and trailing edges with a wedge angle, as is shown with the octagonal profile investigated. The angle of attack plays an important role and in the case of body oscillation, so do the frequency and amplitude of oscillation. Little influence is found to arise from the variation of the Reynolds number in these cases.

For many technical problems of flow-induced oscillations, quasi-steady considerations, deduced from lift and drag characteristics, are sufficient if frequencies are low enough. The measured characteristics of the investigated rectangular and octagonal profile show opposite slopes at zero incidence and accordingly opposite behaviour with respect to movement-induced excitation at low frequencies. Frequency analysis of measured lift forces and flow visualization give evidence that three different classes of vortex formation can be observed with variation of the angle of attack of the profiles: impinging leading-edge vortices, trailing-edge vortex shedding, and alternate-edge vortex shedding.

The unsteady case with profiles oscillating at different amplitudes and frequencies leads to an even larger variety of vortical structures. The response characteristic of the lift force shows resonance in the case of the rectangular profile and almost none for the octagonal profile. Typical for the rectangular profile is a marked jump of the phasing of the fluctuating lift forces relative to the body oscillation at $S_e \approx S^*$ for $\alpha = 0°$.

The phase angle, Θ, between the lift forces and the body oscillation is the most important quantity with respect to the treatment of technical problems, since it allows determination of the ranges of positive energy transfer from the fluid, that is the ranges in frequncy where fluid elastic oscillations of the body are possible. While for the octagonal profile no such ranges can be found, there are two for the rectangular profile, one for very low frequencies (galloping, MIE), and one for resonance with the impinging vortices (IIE). The transition from MIE to IIE is characterized by a continuous decrease of the phase.

A distinct feature of the rectangular profile, oscillating with a mean incidence of $\alpha = 10°$, is that *no* MIE is observed. For $\alpha = 10°$ this profile shows AEVS behaviour with resonance and phase jump at $S_e \approx S_o$.

A coherent statement, through all the experimental data collected, is that the octagonal profile investigated is insensitive to IIE- or MIE-type of induced vibrations.

At high oscillation frequency, fluid inertia effects dominate the magnitude of the fluid forces. This is manifested as a linear increase of the lift forces with growing amplitude of oscillation, for both the rectangular and the octagonal profile.

The main conclusions from the interrelation of the response characteristics of the

rectangular profile, at a constant amplitude of oscillation and the flow viaualizations are as follows.

(i) At very low oscillation frequencies, quasi-steady flow is confirmed and the vortex formation in the wake is not influenced by the body oscillation.

(ii) the resulting vortical structures are synchronized with the body motion in a wide frequency range, in spite of the fact that the flow patterns vary considerably.

(iii) The alteration of the timing in the formation of synchronized vortices at the trailing-edge explains the observed phase jump between the fluctuating lift force and the body oscillation at $S_e \approx S^*$.

(iv) Wake vortex formation is enhanced for resonance at $S_e \approx S_o$ and the formation of impinging leading edge vortices is enhanced for $S_e \approx S^*$.

(v) It is interesting to note that, for the frequency range $S_e \approx S_o$, measurements and flow visualization reveal no abrupt phase change.

(vi) The formation region of the wake decreases with increasing oscillation frequency (within the synchronization range).

(vii) The impingement length of the leading-edge vortices decreases with increasing oscillation frequency.

(viii) Two kinds of vortex coalescence of leading- and trailing-edge vortices are observed, which lead either to an increase or a reduction of the induced lift forces.

(ix) At high oscillation frequency the wavelength of the impinging leading-edge vortices becomes short with respect to the wake width and there is no discernible interaction of these vortices from the lower and upper layers.

The observation that for resonance at $S_e \approx S_o$ no phase jump is observed, while such a jump obviously occurs for $S_e \approx S^*$, remains a topic for future research. The existence of such a phase jump in the lift force or fluctuating pressure relative to the body displacement within the synchronization range is also a point of discussion for the square section cylinder. Measurements on the square section cylinder performed by Bearman & Obasaju (1982) and Nakamura & Mizota (1975) show phase jumps for resonance at $S_e \approx S_o$, while for the same profile Öngören & Rockwell (1988) did not observe a phase jump at $S_e \approx S_o$ in their flow visualization but one at considerably higher frequencies of oscillation.

References

Awbi, H. B. 1983 Effect of blockage on the Strouhal number of two dimensional bluff bodies. *Journal of Wind Engineering and Industrial Aerodynamics* **12,** 353–360.

Bloor, M. S. 1964 The transition to turbulence in the wake of a circular cylinder. *Journal of Fluid Mechanics* **19,** 290–304.

Bearman, P. W. & Luo, S. C. 1988 Investigation of the aerodynamic instability of a square-section cylinder by forced oscillation. *Journal of Fluids and Structures* **2,** 161–174.

Bearman, P. W., Gartshore, I. S., Maull, D. J. & Parkinson, G. V. 1987 Experiments on flow-induced vibration of a square-section cylinder. *Journal of Fluids and Structures* **1,** 19–34.

Bearman, P. W. 1985 Vortex shedding from oscillating bluff bodies. *Annual Review of Fluid Mechanics* **16,** 195–222.

Bearman, P. W. & Obasaju, E. D. 1982 An experimental study of pressure fluctuations on fixed and oscillating square-section cylinders. *Journal of Fluid Mechanics* **119,** 297–321.

Bearman, P. W. & Trueman, D. M. 1972 An investigation of the flow around rectangular cylinders. *Aeronautical Quarterly* **23,** 229–235.

Chaix, B. 1972 Effets d'interférence entre moulinets hydrométriques, supports et parois lors de mesures de débits. Dissertation, Swiss Federal Institute of Technology Lausanne, Juris Verlag Zurich, Switzerland.

DEN HARTOG, J. P. 1934 The vibration problems of engineering. *Proceedings 4 International Congress of Applied Mechanics,* Cambridge, pp. 34–53.
DENIZ, S. 1993 Kräfte auf angeströmte, schwingende Profile mit Rechteck- und Achteckquerschnitt. Dissertation No 10341, Swiss Federal Institute of Technology Zurich, Switzerland.
GERRARD, J. H. 1966. The mechanics of the formation region of vortices behind bluff bodies. *Journal of Fluid Mechanics* **25,** 401–413.
KNISELY, C. W. 1990. Strouhal numbers of rectangular cylinders at incidence: review and new data. *Journal of Fluids and Structures* **4,** 371–393.
NAKAGUCHI, H., HASHIMOTO, K. & MUTO, S. 1968 An experimental study on aerodynamic drag of rectangular cylinders. *Journal of Japan Society for Aeronautical and Space Sciences* **16,** No. 168, 1–5,
NAKAMURA, Y. & OHYA, Y. & TSURUTA, H. 1991 Experiments on vortex shedding from flat plates with square leading edge and trailing edge. *Journal of Fluid Mechanics* **222,** 437–447.
NAKAMURA, Y. & MATSUKAWA, T. 1987 Vortex excitation of rectangular cylinders with a long side normal to the flow. *Journal of Fluid Mechanics* **180,** 171–191.
NAKAMURA, Y. & NAKASHIMA, M. 1986 Vortex excitation of prisms with elongated rectangular, H and L cross-sections. *Journal of Fluid Mechanics* **163,** 149–169.
NAKAMURA, Y. & YOSHIMURA, T. 1982 Flutter and vortex excitation of rectangular prisms in pure torsion in smooth and turbulent flows. *Journal of Sound and Vibration* **84,** 305–317.
NAKAMURA, Y. & MIZOTA, T. 1975 Unsteady lifts and wakes of oscillating rectangular prisms. *ASCE Journal of the Engineering Mechanics Division* **101,** EM6, 855–871.
NAUDASCHER, E. & ROCKWELL, D. 1994 Flow-induced vibration—An engineering guide. Rotterdam: A. A. Balkema.
NAUDASCHER, E. & WANG, Y. 1993 Flow-induced vibrations of prismatic bodies and grids of prisms. *Journal of Fluids and Structures* **7,** 341–373.
ÖNGÖREN, A. & ROCKWELL, D. 1988 Flow structure from an oscillating cylinder—Part 1. Mechanisms of phase shift and recovery in the near wake. *Journal of Fluid Mechanics* **191,** 197–223.
PARKER, R. & WELSH, M. C. 1983 Effects of sound on flow separation from blunt flat plates. *International Journal Heat and Fluid Flow* **4,** 113–127.
PARKINSON, G. V. 1989 Phenomena and modeling of flow-induced vibrations of bluff bodies. *Aerospace Science* **16,** 169–224.
PARKINSON, G. V. 1974 Mathematical models of flow induced vibrations of bluff bodies. In *Flow-Induced Structural Vibrations* (ed. E. Naudascher), pp. 81–127. Berlin: Springer.
ROCKWELL, D. 1990 Active control of globally-unstable separated flows. *ASME Symposium on Non steady Flows* (eds J. A. Miller & D. P. Telionis), Toronto, June, pp. 379–394. New York: ASME.
ROSHKO, A. 1954 On the drag and shedding frequency of two-dimensional bluff bodies. *NACA Technical Note* No. 3169.
RUSCHEWEYH, H. 1988 *Dynamische Windwirkung an Bauwerken,* Vol. 1 and 2. Wiesbaden/Berlin: Bauverlag.
SCRUTON, C. 1981 *Wind effects on structures.* Oxford University Press.
STAUBLI, T. 1983 Untersuchung der oszillierenden Kräfte am querangeströmten, schwingenden Kreiszylinder. Dissertation No 7322, Swiss Federal Institute of Technology Zurich, Switzerland.
THANG, N. D. & NAUDASCHER, E. 1991 Vibration of beams and trashracks in parallel and inclined flows. *ASCE Journal of Hydraulic Engineering* **117,** No 8, 1056–1976.
WASHIZU, K., OHYA, A., OTSUKI, Y. & FUJII, K. 1978 Aeroelastic instability of rectangular cylinders in a heaving mode. *Journal Sound Vibration* **59,** 195–210.

APPENDIX: NOMENCLATURE

A area ($L \times$ span) (m^2)
C_D drag coefficient
C_L lift coefficient
D thickness of the body cross-section (m)
d thickness of the trailing-end (m)
f frequency (Hz)

F force (N)
L length of the body cross-section (m)
Re Reynolds number, equal to VL/ν
S Strouhal number, equal to fD/V
S_e nondimensional excitation frequency
S^* nondimensional frequency of impinging vortices
S_o nondimensional frequency of wake vortex formation
S_o^{ne} nondimensional frequency of wake vortex formation (no excitation)
S_{BG} nondimensional Bloor-Gerrard frequency
T period (s)
V freestream velocity (m/s)
y displacement of the body (m)
α angle of attack (°)
β wedge angle (°)
$\hat{\eta}$ nondimensional amplitude of oscillation, equal to $\hat{y}/D$
θ phase angle between body displacement and lift force
ν kinematic viscosity
ρ density of the fluid
ω angular frequency (rad/s)